Real-Time Flexibility Quantification of a Building HVAC System for Peak Demand Reduction

Guanyu Tian, *Graduate Student Member, IEEE*, Qun Zhou Sun, *Member, IEEE*, and Wenyi Wang

***Abstract*—The quantification of heating, ventilation, and air condition (HVAC) system flexibility is critical to the operations of both the grid and buildings in demand response (DR) programs. However, the flexibility quantification is challenging due to the non-linearity and non-convexity of thermal dynamics associated with HVAC components. This paper proposes a novel HVAC flexibility quantification method based on a semidefinite programming (SDP) formulation. The SDP is reformulated from the non-convex problem of HVAC power optimization, and can be solved efficiently in real-time. The physics-based HVAC model is incorporated to ensure the reliability and accuracy of solutions. The quantification results are organized into an HVAC flexibility table that can provide response strategies on adjusting HVAC setpoints in response to the grid signals received. The developed response strategies minimize occupant discomfort while satisfying grid requirements. A case study of a test building model is carried out to illustrate the flexibility quantification framework and compares the performance of two DR strategies.**

***Index Terms*—HVAC flexibility quantification, demand response, convex optimization.**

I. Introduction

THE power grid is facing increasing uncertainties from high penetration of intermediate renewable energy resources [1]. To mitigate these uncertainties, the demand side plays a critical role to provide flexibilities that are needed by the grid, such as peak shaving and frequency regulation [2]–[4]. Among different types of electrical demand, the thermal controlled loads (TCL) are particularly ideal resources due to their pre-cooling/heating characteristics [5]. The heating, ventilation, and air condition (HVAC) system, which accounts for 44% of the entire electrical load in the US, is the largest TCL power consumer in commercial buildings and is one of the most important Demand Response (DR) resources [6].

The quantification of HVAC flexibility is critical to the effectiveness of DR strategies [7]. Currently, the DR signals are dispatched based on grid information only, such as frequency and line flow [8]. The DR signals should also incorporate the response flexibility of buildings, to avoid mismatches between the expected and actual system states, which could potentially jeopardize the reliability of the grid [9]. For buildings, knowing the power flexibility help determine 1) whether they have the capacity to respond to a specific grid signal and 2) if so, how to efficiently adjust HVAC setpoints to fulfill the grid requirement. If the response flexibility of HVAC systems can be quantified in real-time, the reliability and economics of the grid and building operations can be significantly improved.

Nevertheless, the quantification of HVAC power flexibility is extremely challenging, mainly due to the non-linearity and non-convexity of thermal dynamics associated with HVAC components. Existing methods can be classified into two categories, the linear approximation approaches and simulation model-based approaches.The linear approximation approaches are popular mainly due to their computational efficiency. For example, linearized thermal dynamic model and HVAC power model are incorporated into the flexibility quantification of load providing grid services in [10] and [11]. The linearized models are also widely used in model predictive control (MPC) methods for optimal building operations [12]–[16]. Nevertheless, the approximation error arises during the linearization process and could let the linearized models become impractical under scenarios where high estimation accuracy is required [17]. Efforts of utilizing nonlinear MPC formulations are attempted [18]–[21], but the solutions from nonlinear solvers lack global optimality guarantee [22]. In pursuit of modeling accuracy, the simulation-based methods are adopted. For instance, HVAC power flexibility can be obtained via building simulations developed in EnergyPlus [23], [24]. Modelica, a universal DAE-based simulation platform, can be used to simulate and optimize the control strategy of buildings [25], [26]. Other tools are also available for HVAC simulations, such as TRNSYS and HVACSIM+ [27]. The model-based simulations are developed based on first principle models that are interpretable and potentially more accurate. However, they require extensive modeling efforts, and therefore, are suitable for off-line planning and assessment studies. To obtain an accurate estimation of HVAC flexibility, the simulations are expected to run under actual states collected in real time, which is usually prohibited by extensive modeling effort and heavy computational requirement. Thus, this paper proposes a convex flexibility quantification method that is computationally efficient and can also capture complex physical principles for the applications of HVAC-based DR services.

Another research gap for HVAC-based DR services is the lack of a real-time response strategy to guide the building

Manuscript received 10 June 2021; revised 1 November 2021; accepted 11 December 2021. Date of publication 17 December 2021; date of current version 19 August 2022. This work was supported in part by the U.S. Department of Energy's Office of Energy Efficiency, and Renewable Energy (EERE) under the Building Technology Office, BENEFIT 2019 Award Number DE-EE0009152. Paper no. TPWRS-00929-2021. *(Corresponding author: Qun Zhou Sun.)*

The authors are with the Department of Electrical and Computer Engineering, University of Central Florida, Orlando, FL 32816 USA (e-mail: tiang@knights.ucf.edu; qz.sun@ucf.edu; wenyi.wang@ucf.edu).

Color versions of one or more figures in this article are available at https://doi.org/10.1109/TPWRS.2021.3136464.

Digital Object Identifier 10.1109/TPWRS.2021.3136464

operations throughout a grid event. Given the grid signal and measurements of building states at the moment, building operating conditions, such as HVAC setpoints, need to be adjusted to fulfill the grid power requirement. Finding a proper adjustment is nontrivial. The optimal adjustment varies under different HVAC control schemes. For instance, building controls proposed in [10] and [28] adjust the on/off status of residential HVAC system for load balancing and frequency regulation services. Such control scheme is commonly seen in residential houses but less used in commercial buildings. Adjusting zone temperature setpoints is the most practical response strategy for commercial buildings. In addition to the setpoint of zone temperature, many other variables within the HVAC system can influence the overall power, such as supply air temperature, water pump speed, air fan speed, and supply water temperature. Adjusting zone temperature is straightforward but at the cost of compromising occupant comfort, while adjusting all controllable variables in a coordinated manner may achieve certain amount of flexibility without sacrificing occupant comfort [29]. Expanding the control variables increase the dimension of the problem which presents challenges to develop real-time strategy adjustment.

In this paper, we address these two challenging problems by formulating HVAC DR into a semidefinite programming (SDP) problem. First, an HVAC power minimization problem is formulated under normal operating conditions, where a physics-based HVAC model is adopted. Note that the physics-based HVAC model is nonlinear and non-convex. This paper then proposes approximation and convexification techniques to tackle the original intractable formulation by utilizing SDP. Finally, the convex reformulation is applied in flexibility quantification and response strategy development to guide the operations of HVAC throughout DR periods. Flexibility tables are constructed and proper setpoints are recommended. The formulation is efficiently solvable and can be used in real-time. The results are also compared with nonlinear solver IPOPT to demonstrate the computational efficiency for real-time application.

The contributions of this paper are three folds:

1) *Propose a tractable formulation for the HVAC power minimization problem using SDP:* Specifically, approximation techniques are applied to reduce the nonlinearity of the objective function on power minimization. The approximated problem is then reformulated into an SDP problem to address the bilinear terms in the constraints where supply water mass flow rate and supply water temperature are intertwined.
2) *Propose a real-time HVAC flexibility quantification method:* The HVAC flexibilities are quantified in real-time under different operating conditions. The quantification algorithm is based on the SDP formulation and outputs a flexibility table that shows the power reduction potentials given different setpoints of room temperature and supply air temperature.
3) *Develop a real-time response strategy for HVAC to provide DR:* During DR periods, the optimal setpoints of HVAC variables are critical for buildings to successfully respond to grid signals while minimizing occupant discomforts. The developed algorithm outputs setpoints for room temperature, supply air temperature, supply water mass flow rate, and supply water temperature, which gives real-time response guidance for buildings. The HVAC settings that minimize occupant discomfort can be found efficiently using the flexibility table.

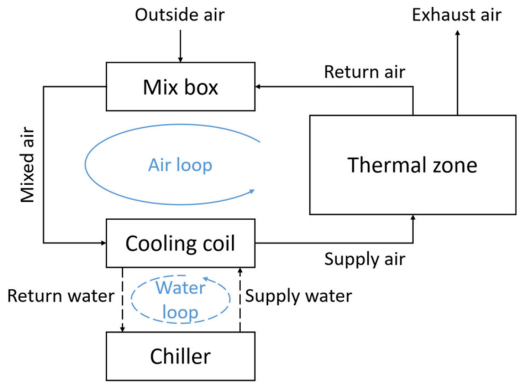

Fig. 1. HVAC system schematic diagram.

This paper is organized as follows. Section II formulates the HVAC power optimization problem under normal conditions. Section III applies approximation and convexification techniques to reformulate the problem into a tractable SDP formulation. Section IV applies the SDP formulation to quantify HVAC flexibility in real-time and provide the optimal setpoints during DR periods. Section V validates the accuracy of the approximation models and shows numerical results of HVAC flexibility quantification and response strategies. The computational efficiency and solution optimality of the proposed SDP formulation is compared to the non-convex formulation solved by the nonlinear solver IPOPT. Section VI discusses the assumptions, potential post-DR surges issue, and future work. Section VII provides conclusions.

II. Optimization for HVAC Operation Under Normal Conditions

A classic formulation of HVAC operation is to minimize power consumption while maintaining occupant comfort. Note that HVAC power consumption comprises that from fans, pumps, and the chiller, while the occupant comfort is related to room temperature. Therefore, HVAC optimization requires detailed modeling of HVAC components, which are presented below. This HVAC formulation is for normal operating conditions, i.e., no grid signals are considered.

A. Structure of HVAC Modeling

Fig. 1 shows the schematic diagram of a typical HVAC system, where the air loop and water loop works simultaneously. The cooling and dehumidifying coil is where the air loop and water loop intersect and exchange heat. The water is driven by pumps and cycles between the coil and chiller in the water loop. The chilled supply water flows into the coil, and the return water goes back to the chiller.

The air passing around the cooling and dehumidifying coil is cooled by the chilled water and circulates inside the air loop by fans. Specifically, the cooled supply air after the coil enters into thermal zones through the supply air fan. After mixing with the air insides the thermal zone, the return air is partly exhausted to the outside, partly circulates back and mixes with the outside air in the mixing box and continues the cycle.

1) Power Modeling: The power consumption of HVAC systems comes from three components: fan, pump, and chiller.

Fan Power: The air flow is driven by fans, and hence, the power consumption of fans is related to the supply air mass flow rate. A commonly used model is a third-order polynomial model formulated in (1), where αs are the coefficients and $\dot{m}_{sa}$ denotes the supply air mass flow rate [30].

$$P_f = \alpha_0 + \alpha_1 \dot{m}_{sa} + \alpha_2 \dot{m}_{sa}^2 + \alpha_3 \dot{m}_{sa}^3 \tag{1}$$

Pump Power: The water flow is driven by pumps, so the power consumption of pumps is related to the supply water mass flow rate. A similar third-order polynomial model in (2) used, where γs are the coefficients and $\dot{m}_{sw}$ denotes the supply water mass flow rate [30].

$$P_p = \gamma_0 + \gamma_1 \dot{m}_{sw} + \gamma_2 \dot{m}_{sw}^2 + \gamma_3 \dot{m}_{sw}^3 \tag{2}$$

Chiller Power: The chiller is where the return water is cooled down and circulates back as supply water. The power consumption of a chiller is related to water mass flow rate, chilled water supply temperature, and condenser water supply temperature. The DOE-2 model in (3) is one of the commonly used chiller power evaluation models [31].

$$P_c = P_{ref} \times CAPFT \times EIRFT \times EIRFPLR \tag{3a}$$

$$CAPFT = a_1 + b_1 T_{sw} + c_1 T_{sw}^2 + d_1 T_{cws} + e_1 T_{cws}^2 + f_1 T_{sw} T_{cws} \tag{3b}$$

$$EIRFT = a_2 + b_2 T_{sw} + c_2 T_{sw}^2 + d_2 T_{cws} + e_2 T_{cws}^2 + f_2 T_{sw} T_{cws} \tag{3c}$$

$$EIRFPLR = a_3 + b_3 PLR + c_3 PLR^2 \tag{3d}$$

$$PLR = \frac{Q}{Q_{ref} CAPFT} \tag{3e}$$

where P_c denotes the actual chiller power, P_{ref} is the reference power in the nominal condition. T_{sw} is chilled water supply temperature. T_{cws} denotes condenser water supply temperature, usually given as a constant input. CAPFT is the capacity ratio, EIRFT is the full load efficiency, and EIRFPLR is the partial load efficiency. PLR is the partial load ratio of the chiller. Q and Q_{ref} are the actual thermal load and the reference thermal load under the nominal condition. More discussions on Q will be presented later in Section II-B. The indexed a, b, c, d, e, and f are coefficients.

2) Thermal Zone Modeling: The thermal zone is modeled using the RC equivalent circuit in Fig. 2 [32]. where the node voltage T_r, T_w, and T_o denote the temperatures of zone, wall, and outside air respectively. R_{wo} and R_{wi} are the exterior and interior thermal resistance of wall. R_{win} is the thermal resistance of window. R_{con} is the convective resistance between the inner surface of wall and room air, and R_{conwin} is that of window. The heat capacity of wall and room air are modeled by the capacitors C_w and C_r. The heat injections from solar irradiance and internal gain are modeled by current sources Q_{rad} and Q_{ig}. $f_{rad,1}, f_{rad,2}$, and $f_{rad,3}$ are the percentages of solar irradiance on different surfaces.

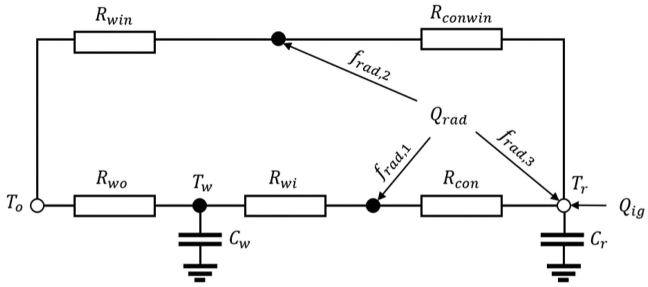

Fig. 2. RC equivalent circuit of thermal zone.

The differential (4a) and (4b) formulates the thermal dynamics of thermal zone and wall [18]. The thermal zone dynamic model (4a) can be further written into the non-linear difference (5) where βs are the aggregated coefficients of physical parameters and T_r, T_w, T_o, and Q_{rad} can be measured in real time.

$$C_r \frac{dT_r}{dt} = \frac{T_o - T_r}{R_{win} + R_{conwin}} + \frac{T_w - T_r}{R_{wi} + R_{con}} + \frac{R_{wi} f_{rad,1} Q_{rad}}{R_{wi} + R_{con}} + \frac{R_{win} f_{rad,2} Q_{rad}}{R_{win} + R_{conwin}} + f_{rad,3} Q_{rad} + Q_{ig} + \dot{m}_{sa} c_{air} (T_{sa} - T_r) \tag{4a}$$

$$C_w \frac{dT_w}{dt} = \frac{T_o - T_w}{R_{wo}} + \frac{T_r - T_w}{R_{wi} + R_{con}} + \frac{R_{con} f_{rad,1} Q_{rad}}{R_{wi} + R_{con}} \tag{4b}$$

$$T_r(t + \Delta t) - T_r(t) = \Delta T_r = \beta_1 \dot{m}_{sa} + \beta_2 \dot{m}_{sa} T_{sa} + \beta_0 \tag{5}$$

Here $T_r(t + \Delta t)$ and $T_r(t)$ denote the room temperature at two adjacent time steps $t + \Delta t$ and t. ΔT_r denotes the room temperature change within a time interval Δt. The analytical formulations of the coefficients are:

$$\beta_0 = -\frac{\Delta t}{C_r} \left(\frac{1}{R_{win} + R_{conwin}} + \frac{1}{R_{wi} + R_{con}} \right) T_r + \frac{\Delta t}{C_r} Q_{ig} + \frac{\Delta t}{C_r (R_{wi} + R_{con})} T_w + \frac{\Delta t}{C_r (R_{win} + R_{conwin})} T_o + \frac{\Delta t}{C_r} \left(\frac{R_{wi} f_{rad,1}}{R_{wi} + R_{con}} + f_{rad,3} + \frac{R_{win} f_{rad,2}}{R_{win} + R_{conwin}} \right) Q_{rad} \tag{6a}$$

$$\beta_1 = -\frac{\Delta t c_{air}}{C_r} T_r \tag{6b}$$

$$\beta_2 = \frac{\Delta t c_{air}}{C_r} \tag{6c}$$

B. HVAC Optimization Formulation

The optimization of HVAC operation under normal conditions is formulated as a power minimization problem in (7).

$$\min_{T_r^{ref},T_{sa}^{ref},\dot{m}_{sa},\dot{m}_{sw},T_{sw}} \quad P_f + P_p + P_c \tag{7a}$$

$$s.t. \quad \dot{m}_{sa}\left(h_{mix} - h_{sa}\right) = Q \tag{7b}$$

$$c_{water}\dot{m}_{sw}\left(T_{rw} - T_{sw}\right) = Q \tag{7c}$$

$$T_r^{next} = T_r + \Delta T_r \tag{7d}$$

$$T_r^{next} \le T_r^{ref} \tag{7e}$$

$$T_{sa} = T_{sa}^{ref} \tag{7f}$$

$$T_r^{lb} \le T_r^{ref} \le T_r^{ub} \tag{7g}$$

$$T_{sa}^{lb} \le T_{sa}^{ref} \le T_{sa}^{ub}$$

$$(1) - (5) \tag{7h}$$

Here the total power consumption of a HVAC system, consisting of power consumed by fan, pump, and chiller, is minimized. (7b) and (7c) are the cooling load balance of the cooling coil from the air and water loops. Q denotes the total cooling load, including both sensible and latent load. For the air loop, Q can be calculated from the enthalpy gap between the mixed air and supply air, i.e. $h_{mix} - h_{sa}$, where enthalpy h is a function of air temperature T and humidity ratio ω formulated in (8).

$$h\left(T,\omega\right) = C_{pa}T + \omega(g_{H_2O} + C_{p\omega}T) \tag{8}$$

where g_{H2O} denotes the evaporation heat of water at $0\,^{\circ}\mathrm{C}$; C_{pa} and C_{pw} are specific heat of air and water at constant pressure [33].

For the air loop side of the coil, inlet air is the mixed air T_{mix} with a humidity ratio of ω_{mix}; the outlet air is the supply air T_{sa} with a humidity ratio of ω_{sa}. For the water loop side of the coil, inlet water is the supply water T_{sw}; the outlet water is the return water T_{rw}. $\dot{m}_{sa}$ and $\dot{m}_{sw}$ denote the mass flow rate of air and water respectively. (7d) and (7e) are the constraints that maintain the room temperature no higher than the room temperature setpoint T_r^{ref}. Constraint (7f) enforces the supply air temperature equals to its setpoint T_{sa}^{ref}. (7g) and (7h) are the constraints that maintain the room temperature and supply air temperature within the upper and lower bounds. This formulation is a common practice that neglects electric dynamics, cooling coil dynamics, and supply air temperature dynamics. These three assumptions will be discussed in Section VI.

III. Water Loop Optimization Using Semidefinite Programming

Note that the room temperature and supply air temperature (T_r and T_{sa}) have a direct impact on occupant comfort, so they should be handled with extra caution. For now, we assume their setpoints are fixed, and their flexibility will be discussed in later Sections. In formulation (7), to obtain the minimum power of the entire HVAC system, the expected zone temperature at the next step must be binding to its upper bound, i.e., constraint (7e) becomes an equality constraint. Then the optimal solution of air mass flow rate $\dot{m}_{sa}^{*}$ can be calculated directly from (5) by letting $\Delta T_r = T_r^{ref} - T_r$ and $T_{sa} = T_{sa}^{ref}$. As a result,

$$\dot{m}_{sa}^{*} = \min\left(\dot{m}_{sa}^{ub}, \max\left(\dot{m}_{sa}^{lb}, \frac{T_r^{ref} - T_r - \beta_0}{\beta_1 + \beta_2 T_{sa}^{ref}}\right)\right) \tag{9}$$

Note that $T_r(t + \Delta t)$ is set to be the setpoint T_r^{ref} to derive the optimal control of $\dot{m}_{sa}$. $T_r(t)$ denotes the real-time measurement of room temperature. For simplicity, the time indices t and $t + \Delta t$ are omitted. $\dot{m}_{sa}^{lb}$ and $\dot{m}_{sa}^{ub}$ are the lower and upper bounds of air mass flow rate. Given the supply air mass flow rate $\dot{m}_{sa}^{*}$, the fan power P_f can be explicitly computed using (1). By doing so, the air loop and the water loop are essentially decoupled. Now, the HVAC optimization problem (7) is reduced to a water loop optimization formulated in (10) under fixed T_r^{ref} and T_{sa}^{ref}.

$$\min_{m_{sw},T_{sw}} \quad P_p + P_c \tag{10a}$$

$$s.t. \quad c_{water}\dot{m}_{sw}\left(T_{rw} - T_{sw}\right) = Q \tag{10b}$$

$$\dot{m}_{sw}^{lb} \le \dot{m}_{sw} \le \dot{m}_{sw}^{ub} \tag{10c}$$

$$T_{sw}^{lb} \le T_{sw} \le T_{sw}^{ub} \tag{10d}$$

Constraint (10b) denotes the energy balance that transfers the cooling load of air loop to the water loop, where $Q = \dot{m}_{sa}^{*}(h_{mix} - h_{sa}^{ref})$. Constraint (10c) and (10d) limit the boundaries of the decision variables.

Due to the non-convexity from both the objective (10a) and constraint (10b), the water loop optimization problem (10) is not efficiently solvable. Although it could be solved using gradient-based methods or global optimization solvers, the solution of the former has no global optimality guarantee, while the latter is usually computationally expensive.

To improve the optimality and computational efficiency, approximation and relaxation techniques are employed. First, the pump and chiller power models are approximated using lower-order polynomials by minimizing the modeling errors. Then semidefinite programming (SDP) is applied to the water loop optimization problem. This convex formulation can be solved efficiently and employed in real-time flexibility quantification.

A. Quadratic Approximations of Water Loop Power Models

Despite the physical principles in the overall HVAC model, the power models for pump and chiller are mostly data-driven high-order polynomial regressions. To maintain tractability, the power models are approximated using quadratic functions, with the goal of minimizing modeling mismatch from the original high-order polynomial functions.

1) Pump: The approximation model of pump is formulated in (11) and its optimal coefficients $\hat{\gamma}_0, \hat{\gamma}_1$, and $\hat{\gamma}_2$ can be analytically obtained. The project theorem is applied to find the approximated coefficients $\hat{\gamma}_0, \hat{\gamma}_1$, and $\hat{\gamma}_2$ that minimize the error $\|P_p - \hat{P}_p\|$. The derivation is given in Appendix A.

$$\hat{P}_p = \hat{\gamma}_0 + \hat{\gamma}_1\dot{m}_{sw} + \hat{\gamma}_2\dot{m}_{sw}^2 \tag{11}$$

Fig. 3 shows the comparison between the original third-order model and the approximated second-order model within the

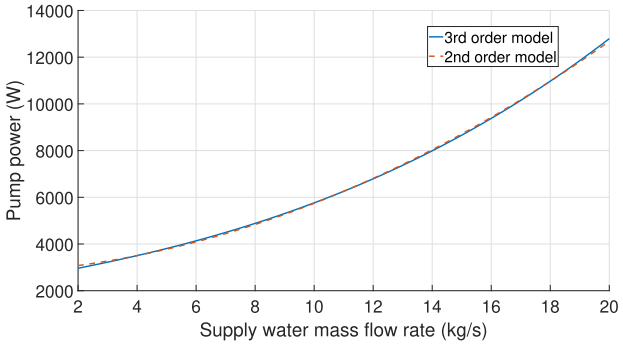

Fig. 3. Pump power approximation.

operational ranges of $\dot{m}_{sw} \in [2, 20]$, indicating close proximity between the two models.

2) Chiller: Unfortunately, the DOE2 model for chiller power is in a much higher order and hence it is difficult to obtain an analytical solution. However, note that its surface within the operational region of $\dot{m}_{sa}$ and T_{sw} is a skewed hyperbolic paraboloid. Therefore, the DOE-2 model can be approximated by a second-order polynomial model in (12).

$$\begin{aligned}\hat{P}_c &= X_c^T \Theta X_c + \theta^T X_c + \theta_0 \\ &= \Theta_{11} m_{sw}^2 + \Theta_{22} T_{sw}^2 + \Theta_{33} T_{rw}^2 \\ &\quad + 2\Theta_{12} m_{sw} T_{sw} + 2\Theta_{13} m_{sw} T_{rw} + 2\Theta_{23} T_{sw} T_{rw} \\ &\quad + \theta_1 m_{sw} + \theta_2 T_{sw} + \theta_3 T_{rw} + \theta_0 \end{aligned} \tag{12}$$

where $X_c = [m_{sw}, T_{sw}, T_{rw}]^T$ is the vector of chiller power model variables, $\Theta \in R^{3\times 3}$ is the symmetrical matrix that denotes the coefficients of the quadratic terms, $\theta \in R^3$ is the coefficient vector of the linear terms and θ_0 is the constant term.

When approximating the chiller power in real time, (12) can be reduced to (13), where the coefficients of the first-order terms are shown in (14).

$$\begin{aligned}\hat{P}_c &= \Theta_{11} m_{sw}^2 + \Theta_{22} T_{sw}^2 + 2\Theta_{12} m_{sw} T_{sw} + \hat{\theta}_1 m_{sw} \\ &\quad + \hat{\theta}_2 T_{sw} + \hat{\theta}_0 \end{aligned} \tag{13}$$

$$\begin{aligned}\hat{\theta}_0 &= \theta_0 + \theta_3 T_{rw} + \Theta_{33} T_{rw}^2 \\ \hat{\theta}_1 &= \theta_1 + 2\Theta_{13} T_{rw} \\ \hat{\theta}_2 &= \theta_2 + 2\Theta_{23} T_{rw} \end{aligned} \tag{14}$$

Chiller power within operational ranges is generated from the DOE-2 model as synthetic data. Then the coefficients of the approximated model that minimizes the error $\|P_c - \hat{P}_c\|$ can be fitted.

Fig. 4 shows an example of the DOE-2 model and the approximated second-order model surfaces within the operational ranges of $\dot{m}_{sw} \in [2, 20]$ and $T_{sw} \in [4, 10]$ under $T_{rw} = 12$. Fig. 5 shows the contour map of the two models from 12 kW to 200 kW with a 10 kW interval. The results indicate that the second-order polynomial approximation is acceptable in practice.

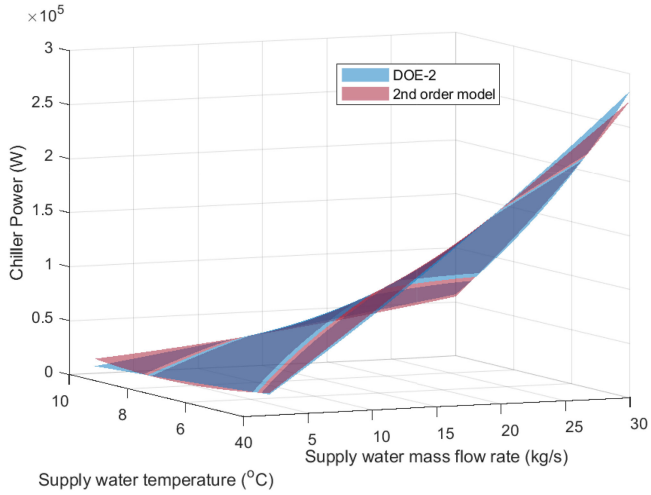

Fig. 4. Chiller power approximation.

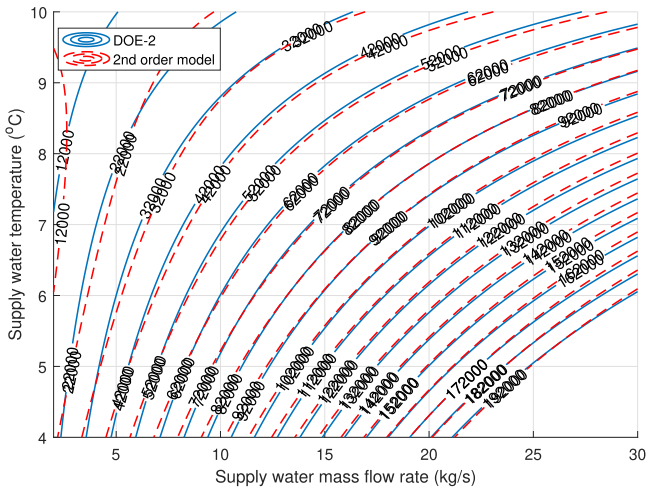

Fig. 5. Chiller power approximation with contour map.

B. SDP Reformulation

The approximated models (11) and (13) are employed to substitute the originals in the objective function of (10). The approximated problem is then re-formulated into an optimization problem with quadratic equality constraints using change-of-variables, which is further relaxed into a convex SDP where a global optimal solution can be obtained efficiently.

The optimization of water loop power with approximated pump and chiller models is formulated in (15), where the non-convexity comes from the quadratic term $\dot{m}_{sw} T_{sw}$ in (15b).

$$\begin{aligned}\min_{m_{sw}, T_{sw}} \quad & \left(\Theta_{11} + \hat{\gamma}_2\right) m_{sw}^2 + \Theta_{22} T_{sw}^2 + 2\Theta_{12} m_{sw} T_{sw} \\ & + \left(\hat{\theta}_1 + \hat{\gamma}_1\right) m_{sw} + \hat{\theta}_2 T_{sw} + \hat{\theta}_0 + \hat{\gamma}_0 \end{aligned} \tag{15a}$$

$$\begin{aligned} s.t. \quad & c_{water} \dot{m}_{sw} \left(T_{rw} - T_{sw}\right) = Q \\ & (10c), (10d) \end{aligned} \tag{15b}$$

Applying the change of variable technique, we can further reformulate this problem. Let $X = [\dot{m}_{sw} \quad T_{sw} \quad 1]^T$, and $W \in \mathbb{R}^{3\times 3}$ be a positive semidefinite matrix defined in (16).

$$W = XX^T = \begin{bmatrix} \dot{m}_{sw}^2 & \dot{m}_{sw}T_{sw} & \dot{m}_{sw} \\ \dot{m}_{sw}T_{sw} & T_{sw}^2 & T_{sw} \\ \dot{m}_{sw} & T_{sw} & 1 \end{bmatrix} \tag{16}$$

Formulation (15) can be equivalently written into (17), where the subscription of W denotes the row and column indexes of an element. Constraint (17e)-(17h) guarantees the invertibility of W to X. The non-convexity of (17) lies in the quadratic equality constraints (17f)-(17h).

$$\min_{W} \left(\Theta_{11} + \hat{\gamma_2}\right) W_{11} + \Theta_{22}W_{22} + 2\Theta_{12}W_{12} + \left(\hat{\theta}_1 + \hat{\gamma_1}\right) W_{13} + \hat{\theta}_2 W_{23} + \hat{\theta}_0 + \hat{\gamma_0} \tag{17a}$$

$$s.t. \quad c_{water}T_{rw}W_{13} - c_{water}W_{12} = Q \tag{17b}$$

$$\dot{m}_{sw}^{lb} \le W_{13} \le \dot{m}_{sw}^{ub} \tag{17c}$$

$$T_{sw}^{lb} \le W_{23} \le T_{sw}^{ub} \tag{17d}$$

$$W_{33} = 1 \tag{17e}$$

$$W_{11} = W_{13}^2 \tag{17f}$$

$$W_{22} = W_{23}^2 \tag{17g}$$

$$W_{12} = W_{13}W_{23} \tag{17h}$$

Given $W \succcurlyeq 0$ and (17e), it can be proofed that (17h) is redundant and can be removed. The proof is provided in Appendix B. With out loss of global optimality, the equality constraints (17f) and (17g) can be relaxed into the inequality constraints (18). Because the inequality constraints define the lower bounds of W_{11} and W_{22}. Considering the coefficients of W_{11} and W_{22}, $\Theta_{11} + \hat{\gamma_2}$ and Θ_{22}, are both positive, (18) and (19) must be binding under the optimal solution. Hence, the equality constraints (17f) and (17g) must hold for the optimal solution.

$$W_{11} - W_{13}^2 \ge 0 \tag{18a}$$

$$W_{22} - W_{23}^2 \ge 0 \tag{18b}$$

By the Shur's complementary, the original problem (15) is equivalently reformulated into the SDP in (19), where the linear matrix inequality (LMI) constraints (19b) and (19c) guarantee that W is a positive semidefinite matrix. The optimal solution of original formulation (15) can be obtained by solving the SDP problem (19), which is more efficient and has global optimality.

$$SDP: \min_{W} \left(\Theta_{11} + \hat{\gamma_2}\right) W_{11} + \Theta_{22}W_{22} + 2\Theta_{12}W_{12} + \left(\hat{\theta}_1 + \hat{\gamma_1}\right) W_{13} + \hat{\theta}_2 W_{23} + \hat{\theta}_0 + \hat{\gamma_0} \tag{19a}$$

$$s.t. \quad \begin{bmatrix} W_{11} & W_{13} \\ W_{13} & 1 \end{bmatrix} \succcurlyeq 0 \tag{19b}$$

$$\begin{bmatrix} W_{22} & W_{23} \\ W_{23} & 1 \end{bmatrix} \succcurlyeq 0 \tag{19c}$$

$$(17b), (17c), (17d), (17e) \tag{19d}$$

Algorithm 1: HVAC Flexibility Quantification.

Input: $\{T_r^{ref,i}, \forall i\}, \{T_{sa}^{ref,j}, \forall j\}, T_r, T_w, T_{rw}$
Output: $\{P_{flex}^{i,j}, \forall i, j\}$

```
Quantify baseline power:
  P^nom = SDP(T_r^nom, T_sa^nom, T_r, T_w, T_rw);
for i = 1 to N do
    for j = 1 to M do
        Quantify HVAC power:
          P^{i,j} = SDP(T_r^{ref,i}, T_sa^{ref,j}, T_r, T_w, T_rw);
        Calculate power reduction:
          P_flex^{i,j} = P^nom − P^{i,j};
    end
end
```

TABLE I
SIMPLE EXAMPLE OF HVAC FLEXIBILITY TABLE

P_{flex} (T_{sa}^{ref} / T_r^{ref})	14 °C	16 °C	18 °C
21 °C	20.20 (20.60-0.40)	0.00 (0.00+0.00)	-64.52 (-64.90+0.38)
22 °C	64.07 (42.24+21.83)	63.46 (41.00+22.46)	61.06 (37.98+23.08)
23 °C	64.19 (42.28+21.91)	63.61 (41.06+22.55)	61.28 (38.11+23.17)

IV. REAL-TIME HVAC FLEXIBILITY QUANTIFICATION AND RESPONSE STRATEGY

The SDP formulation (19) solves for the optimal operating variables of water mass flow rate $\dot{m}_{sw}$ and supply water temperature T_{sw} as well as the minimum power obtained under normal conditions, i.e., the setpoints of room temperature and supply air temperature are fixed. In the case of responding to DR events, these setpoints can be adjusted to provide flexibility to the grid. Such flexibility can be quantified in real-time using the SDP formulation in Section III. The quantified flexibility can also provide a response strategy for setting up the optimal values of these setpoints upon receiving grid signals.

A. Real-Time HVAC Flexibility Quantification

The setpoints under nominal conditions are denoted as T_r^{nom} and T_{sa}^{nom}. The HVAC power under the nominal conditions P^{nom} is computed as the baseline with input measurements of current states, including room temperature T_r, wall temperature T_w, and return water temperature T_{rw}. Any power deviations by adjusting T_r^{ref} and T_{sa}^{ref} are considered as the flexibility P_{flex}. To quantify such flexibility given the range of adjustment, $T_{sa}^{ref} \in [T_{sa}^{lb}, T_{sa}^{ub}]$ and $T_r^{ref} \in [T_r^{lb}, T_r^{ub}]$, SDP could be run repetitively under different settings with the real-time building measurements.

Algorithm 1 describes the HVAC flexibility quantification process, where N and M are the number of setpoint values of T_r^{ref} and T_{sa}^{ref}. $SDP(T_r^{ref,i}, T_{sa}^{ref,j})$ denotes solving the proposed SDP formulation under the setpoints of the i^{th} discretized value of T_r^{ref} and the j^{th} value of T_{sa}^{ref}.

Algorithm 2: Search Of The Optimal Response Strategy.

Input: $P_{DR}, \{P_{flex}^{i,j}, \forall i,j\}, T_r, T_w, T_{rw}$
Output: $T_r^{ref^*}, T_{sa}^{ref^*}, \dot{m}_{sa}^*, \dot{m}_{sw}^*, T_{sw}^*$
for *i = 1 to N* **do**
  Find the largest entry in the i^{th} row $P_{flex}^{max,i} = \max\{P_{flex}^{i,j}, \forall j\}$;
  if *Exist feasible solution, i.e.,* $P_{flex}^{max,i} \geq P_{DR}$ **then**
    Optimal solution found $T_r^{ref^*} = T_r^{ref,i}$;
    $T_{sa}^{ref^*} = \text{argmin}\{|\ T_{sa}^{ref,j} - T_{sa}^{nom}\ |: P_{flex}^{max,i} \geq P_{DR}\}$
    Calculate $\dot{m}_{sa}^*$ from (9)
    $\dot{m}_{sw}^*, T_{sw}^* = SDP(T_r^{ref^*}, T_{sa}^{ref^*}, T_r, T_w, T_{rw})$
    Return $T_r^{ref^*}, T_{sa}^{ref^*}, \dot{m}_{sa}^*, \dot{m}_{sw}^*, T_{sw}^*$
  end
end

TABLE II
MODEL PARAMETERS

	Parameter	Value	Parameter	Value
Fan power coefficients	α_0	3157	α_1	322.2
	α_2	1.131	α_3	0.846
Pump power coefficients	γ_0	2498	γ_1	216.8
	γ_2	7.037	γ_3	0.393
Chiller power coefficients	a_1	0.9830684	a_2	0.6228513
	a_3	0.03295553	b_1	0.03676199
	b_2	-0.008700783	b_3	0.9114398
	c_1	5.307995e-05	c_2	0.0009719796
	c_3	0.05565265	d_1	-0.004828624
	d_2	0.005184584	e_1	-4.755963e-05
	e_2	0.0004951699	f_1	-0.0002377982
	f_2	-0.0014448555		
Physical constants	c_{air}	1014.54 J/(kg°C)	c_{water}	4184 J/(kg°C)
	Δt	1/12 h		
Building parameters	R_{win}	1e-6 °C/W	R_{conwin}	0.000195 °C/W
	R_{con}	0.000048 °C/W	R_{wi}	0.000019 °C/W
	C_r	36219078 J/°C	$f_{rad,1}$	0.759 °C/W
	$f_{rad,2}$	0.151 °C/W	$f_{rad,3}$	0.09 °C/W
HVAC capacity	P_{ref}	91918.5 W	Q_{ref}	383300 J

As a result, a flexibility table can be obtained. Table I gives an example of the HVAC flexibility table, where the rows are different setpoints of T_r^{ref}, and the columns denote the setpoints of T_{sa}^{ref}. T_r^{nom} and T_{sa}^{nom} are 21 °C and 16 °C respectively. The entries of the table denote the HVAC power flexibility that consist of fan power reduction and water-loop power reduction. The contributions of these two parts are denoted in the brackets below the entries separately. One can see that when room temperature and supply temperature are not adjusted, the flexibility is 0. When T_r^{ref} is increased to 22 °C and T_{sa}^{ref} remains at 16 °C, the HVAC can provide up to 63.46 kW power reduction, which includes 41 kW from fan power reduction and 22.46 kW from water-loop power reduction. Further reducing T_{sa}^{ref} from 16 °C to 14 °C, the flexibility is increased to 64.07 kW, including 42.24 kW from fan and 21.83 kW from water-loop.

There are two flexibility values worth mentioning: $P_{flex}^{max,1}$ and P_{flex}^{max}. $P_{flex}^{max,1}$ is the largest entry of the first row in the flexibility table, denoting the largest flexibility that can be achieved while keeping the same room temperature setpoint T_r^{ref}. P_{flex}^{max} is the largest entry of the entire flexibility table, denoting the maximum power reduction can be provided by HVAC by adjusting both room and air temperature setpoints. These two critical values provide guidance for buildings to find optimal adjustment when responding to grid signals, which will be depicted below.

B. Real-Time HVAC Response Strategy

Upon receiving grid DR signals P_{DR}, the optimal response setpoints can be found efficiently from the HVAC flexibility table, where a lower T_r^{ref} deviation is the first priority to ensure occupant comfort, and a low deviation of T_{sa}^{ref} is the second priority. The feasible solutions are in the area where $P_{flex}^{i,j}$ is no less than P_{DR}. i and j denote the index of room temperature and supply air temperature setpoints. The searching process is described in Algorithm 2.

Here the $T_r^{ref^*}$ and $T_{sa}^{ref^*}$ denote the optimal solution of room temperature and supply air temperature setpoints. $P_{flex}^{max,i}$ is the maximum power reduction in the i^{th} row that corresponding to $T_r^{ref,i}$. Due to the monotonicity of HVAC power to T_r^{ref}, we search $P_{sa}^{max,i}$ from current room condition T_r^{nom} to the upper bound of room temperature setpoint T_r^{ub}, and the first row that contains feasible solution yields the minimum room temperature deviation. Then the optimal supply air temperature setpoint $T_{sa}^{ref^*}$ is the feasible solution that yields the lowest supply air temperature deviation in that row. Given $T_r^{ref^*}$ and $T_{sa}^{ref^*}$, the optimal air mass flow rate $\dot{m}_{sa}^*$ can be obtained analytically using (9), and the optimal water mass flow rate $\dot{m}_{sw}$ and supply water temperature T_{sw} can be obtained by solving the SDP.

C. Complexity Analysis

Consider the quantification of HVAC power consumption under one specific setpoint as a unit operation, i.e., one SDP solve is a unit operation. The complexity of constructing the flexibility table is $O(MN)$. For instance, when $T_r \in [21, 25]$ and $T_{sa} \in [14, 18]$ with a granularity of 0.1 °C, $N = 40$ and $M = 40$. It takes 1600 unit operations to construct the flexibility table. Hence the computational efficiency of the quantification algorithm is crucial to the real-time application. The time consumption of the proposed SDP is 0.02 seconds per solve and the total time of constructing the flexibility table is less than 1 minute. In contrast, the solution time of nonlinear optimization solvers, such as IPOPT for the original non-convex formulation, is not sufficiently fast for real-time application. Details about the computation time test are presented in Section V.

V. CASE STUDY

In this Section, the proposed HVAC flexibility quantification and DR strategy are tested using a zone model with the parameters summarized in Table II. The rated HVAC capacity and coefficients of fan, pump, and chiller power models are obtained from and calibrated according to the manufacture provided performance curves [31]. The building parameters are estimated according to the building size and materials from the typical unit values [33], [34]. In practice, these parameters can also be obtained by applying regression methods on data from building automation systems. The outside air temperature profile is a

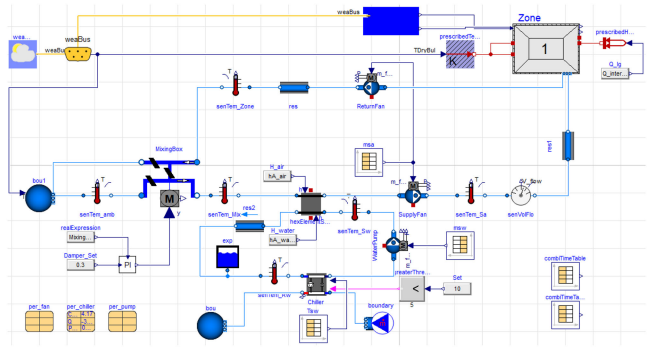

Fig. 6. Layout of the test system.

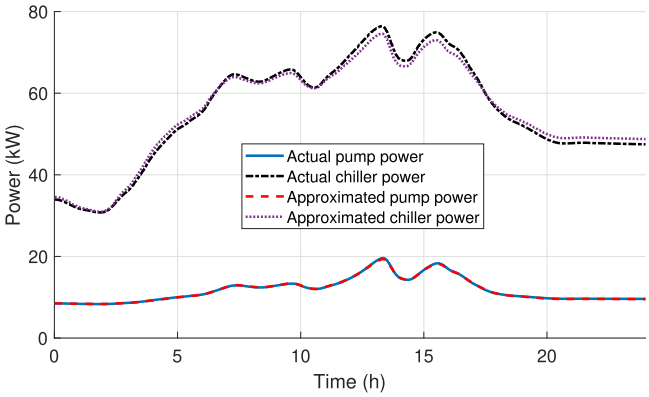

Fig. 7. Comparison of actual and approximated pump and chiller power profiles.

typical summer day weather profile. The SDP is solved using Mosek in Python, on a desktop with a 4-core 3.2 GHz CPU and 8 GB RAM.

A. Validation of Power Approximation Models

A dymola model is established to validate the power approximation models with nominal setpoints ($T_r^{nom} = 21\,^{\circ}\mathrm{C}$ and $T_{sa}^{nom} = 16\,^{\circ}\mathrm{C}$), as shown in Fig. 6. Fig. 7 shows the comparison of actual power profiles from Dymola and quantified power profiles using approximation models. The Root Mean Squared Error (RMSE) of pump and chiller are 0.0608 kW and 1.1311 kW respectively. The pump approximation model is more accurate than chiller by adopting the project theorem, though the approximation error of chiller is also acceptable with its relative error less than 1%.

B. HVAC Flexibility Quantification

The response ranges of room temperature T_r^{ref} and supply air temperature setpoints T_{sa}^{ref} are $[21, 23]$ and $[14, 18]$ respectively. The setpoints can be adjusted every $0.1\,^{\circ}\mathrm{C}$. As a result, the numbers of discrete setpoint values are $N = 21$ and $M = 41$, and hence the flexibility table has 21 rows and 41 columns. Due to the large size of the flexibility table, the quantification results are presented in the form of heat maps. Fig. 8 and Fig. 9 show the heat map of flexibility tables at 6 a.m. and 9 a.m. respectively,

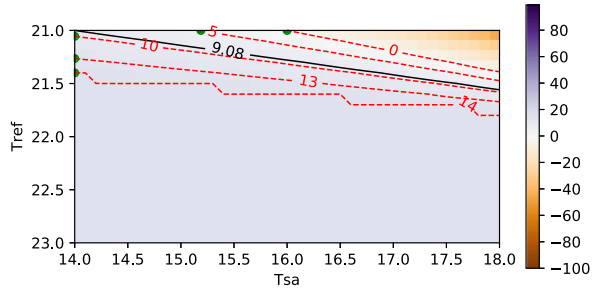

Fig. 8. Heat map of HVAC flexibility table at 6 a.m.

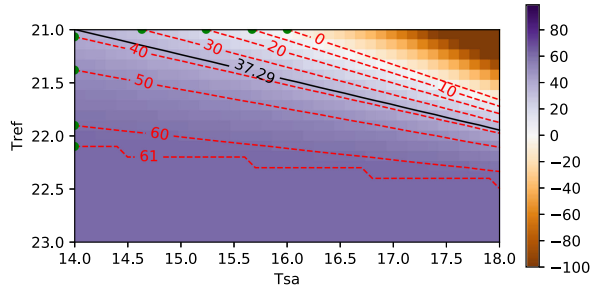

Fig. 9. Heat map of HVAC flexibility table at 9 a.m.

where the vertical axis denotes the room temperature setpoint and the horizontal axis denotes the supply air temperature setpoint. The power flexibility or reduction potential is represented by different colors. The dashed lines are the contours of P_{flex}, and the optimal response strategies are denoted by the circle markers which indicate minimum deviation of room temperature and supply air temperature from its nominal values. The solid line is the boundary of the two regions with and without the need for T_r^{ref} adjustment.

Clearly, the HVAC presents different flexibilities at different times. The maximum response capacity at 6 a.m. is 14.35 kW, achieved at $T_{sa}^{ref} = 14\,^{\circ}\mathrm{C}$ and $T_r^{ref} \geq 21.4\,^{\circ}\mathrm{C}$. In contrast, the maximum response capacity at 9 a.m. is 61.88 kW, achieved at $T_{sa}^{ref} = 14\,^{\circ}\mathrm{C}$ and $T_r^{ref} \geq 22.1\,^{\circ}\mathrm{C}$. It is observed that 9 a.m. has higher flexibility because the outside air temperature and nominal HVAC power are higher, so the gap to the power lower bound is larger. The flexibility tables provides guidance for optimal DR to buildings when receiving grid signals.

C. HVAC Response to Grid Signals

The DR signals are shown in Fig. 10, where the first signal is to reduce 20 kW in the period of 9 a.m. to 11 a.m., the second signal is to reduce 50 kW in the period of 2 p.m. to 6 p.m.

Two strategies are tested to respond to such grid signals. The first strategy is a traditional method that adjusts room temperature setpoint only, labeled as strategy 1, and the second strategy adjusts both room temperature and supply air temperature setpoint, labeled as strategy 2.

The profiles of nominal power, target power, and HVAC power using the two strategies are quantified in Fig. 11, where the power profile of strategy 2 better tracks the target power profile.

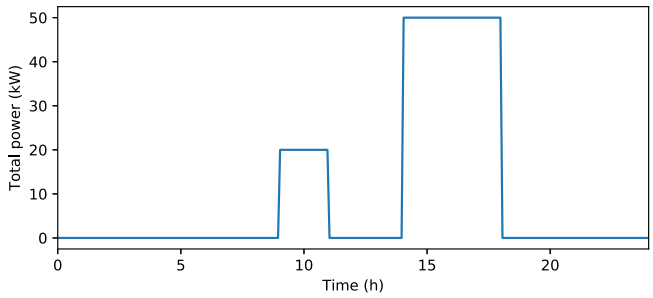

Fig. 10. Demand response signal profile.

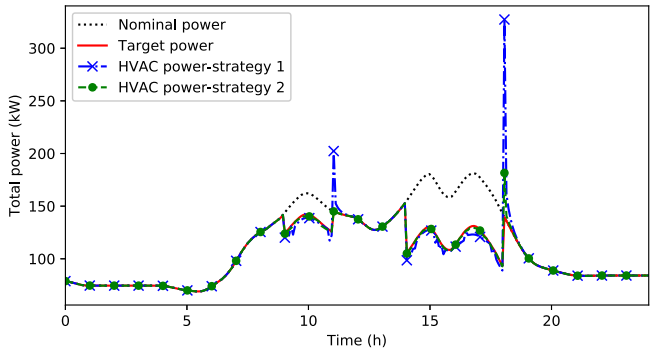

Fig. 11. HVAC total power profiles.

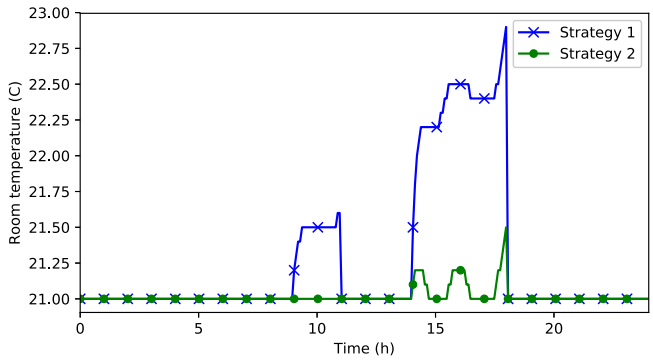

Fig. 12. Room temperature profiles.

It indicates that two-dimensional adjustment in both temperature setpoints provides a more accurate response to the grid signals. Note that both strategies may cause post-DR power spikes when the DR signals end. This is common aftermath for thermal loads because the room temperature is raised during the DR period, and HVAC needs to consume more power to bring the room temperature back to the nominal values. However, the spike of strategy 2 is lower because the room temperature deviation is minimized during the DR period. The issue of post-DR power surges will be further discussed in Section VI.

Fig. 12 shows the room temperature profiles of the two strategies, where strategy 2 yields less room temperature deviation in both DR periods and maintains the nominal room temperature in the first DR period. Strategy 1 raises the room temperature

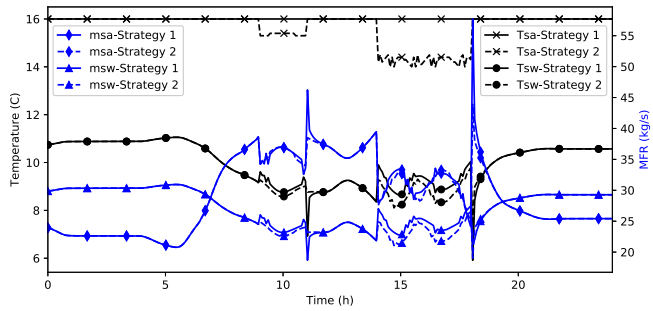

Fig. 13. Profiles of supply air temperature, air mass flow rate, water mass flow rate, and supply water temperature under the two strategies.

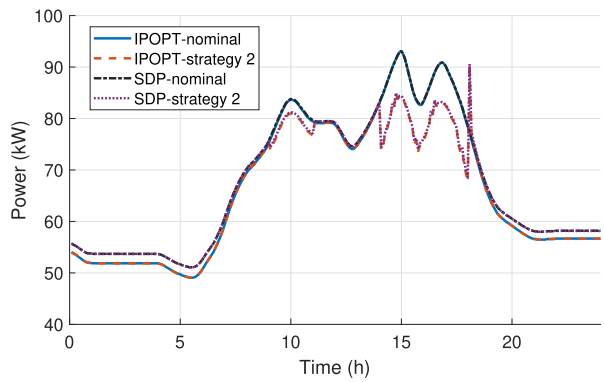

Fig. 14. Comparison of optimal power solved by IPOPT and SDP.

by approximately $0.5\,^{\circ}\mathrm{C}$ and $2.5\,^{\circ}\mathrm{C}$ during the two DR periods, which negatively impacts occupant comfort.

Fig. 13 shows the profiles of the remaining variables, including supply air temperature (cross markers), air mass flow rate (diamond markers), water mass flow rate (triangle markers), supply water temperature (circle markers) under the two strategies. The solid lines are the results of strategy 1, and the dashed lines are from strategy 2. The left y-axis is the reference for temperature profiles and the right y-axis is the reference for mass flow rate profiles. These profiles provide buildings a real-time guide for the setpoint adjustment to effectively respond to grid energy requirements.

D. Computational Efficiency and Solution Optimality

The solution of SDP is a global optimal solution to the approximated water-loop power model. A nonlinear solver IPOPT is now applied to the original non-convex model for comparison. Fig. 14 shows the minimum water-loop power quantified by IPOPT and SDP under nominal setpoints and strategy 2. The largest solution gap in nominal conditions is approximately 2 kW (2.5%) and the largest gap during the DR periods are 0.4598 (0.6%) kW and 0.8563 (1.1%) kW under nominal setpoints and strategy 2 respectively. The two formulations present results that are sufficiently close to each other in the DR applications.

The main advantage of the proposed SDP is its high computational efficiency. The per-step run-time are recorded and summarized into the two histograms in Fig. 15. The average run

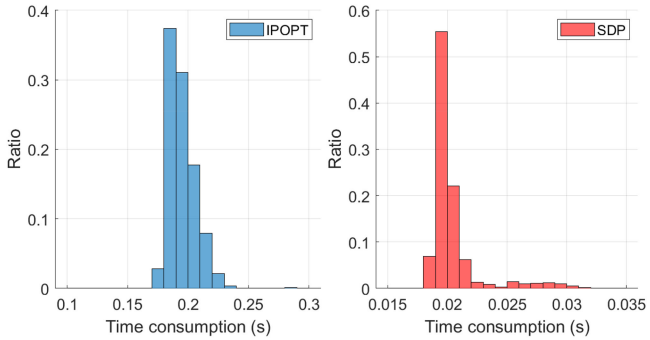

Fig. 15. Comparison of solving time per scenario used by IPOPT and SDP.

time of IPOPT is 0.2008 seconds with a standard deviation of 0.1419, while the average run time of SDP is 0.0204 seconds with a standard deviation of 0.0024. SDP is 10 times faster than IPOPT, making real-time quantification feasible. The standard deviation of SDP is also lower than IPOPT, indicating the run time of SDP is more reliable.

VI. Discussion

This work is our first attempt that applies semidefinite programming (SDP) to the quantification of HVAC power flexibility. It is aimed to pave the way for HVAC system participation in DR services and electricity markets. This Section is to discuss the areas of improvement for the proposed techniques, including modeling assumptions and post-DR surges, as well as extensions and other potential applications.

A. Modeling Assumptions

Three assumptions have been made for the modeling of HVAC components. These assumptions could be explored further to improve the HVAC model.

First, the dynamics of electric components, such as the transient of motors of fan, pump, and compressor are assumed to be negligible. This reflects in the power models (1)-(3). This assumption is commonly adopted in the literature of grid-interactive efficient buildings [11], [35], [36]. The response time of electric power transient is at the second-level and below, much less than the minute-level thermal dynamics of air and thus neglected.

Second, the thermal capacitance of cooling and dehumidifying coil tube is regarded to be zero, i.e., the transient of thermal transfer at the coil is neglected. This applies to constraint (7b) and (7c). This assumption is made based on the fact that the heat capacitance of water ($4182 J/(kg\,^\circ\mathrm{C})$) and air ($1014.54 J/(kg\,^\circ\mathrm{C})$) are much larger than that of metals, such as copper ($0.386 J/(kg\,^\circ\mathrm{C})$). Hence, the heat transfer between water and air is assumed instant.

Third, the dynamics of supply air temperature is neglected, i.e., T_{sa} is assumed to be able to converge to its setpoint T_{sa}^{ref} very quickly. This is observed from simulation data. Fig. 16 shows examples of T_{sa} transient dynamics, where its setpoint is changed from $16\,^\circ\mathrm{C}$ to $15.5\,^\circ\mathrm{C}$, $15\,^\circ\mathrm{C}$, and $14.5\,^\circ\mathrm{C}$ at the 50th minute. The new setpoint can be achieved and stabilized within one minute.

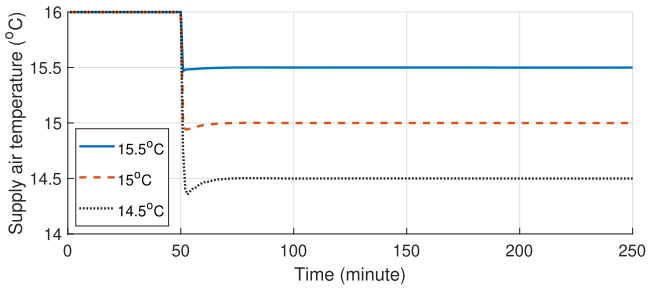

Fig. 16. Examples of supply air temperature transient dynamics.

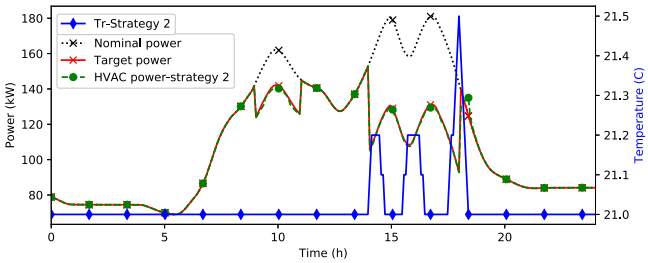

Fig. 17. Profiles of HVAC power and room temperature with post-DR surge buffer.

B. Post-DR Surges

The post-DR power surges are observed in our case studies, due to that HVAC attempts to restore the pre-DR room temperature setpoint as quickly as possible. This could potentially cause high energy costs. One solution is to add a buffer following peak-shaving events by gradually ramping down the room temperature setpoint. Fig. 17 shows that the post-DR spikes are effectively reduced using a $-0.1\,^\circ\mathrm{C}$ per step ramp limit, while the room temperature is restored after 25 minutes. One can see that it takes a longer time for room temperature to recover with such a scheme. A holistic approach to consider costs while responding to DR signals could be further developed.

C. Extensions and Other Applications

The proposed SDP formulation only considers the cooling mode. More practical HVAC models including air handling unit, variable air volume box, and reheating coil can be further incorporated. In addition, extending to heating mode could be explored with a similar heat balance equation as in (15b), except that the supply water temperature T_{sw} is higher than return water temperature T_{rw}. The power model of boilers can be either modeled using constant Coefficient of Performance (COP) or approximated with a second-order polynomial function of m_{sw} and T_{sw} and the approximation accuracy also needs further investigation.

Following this preliminary work, we also intend to expand the SDP formulation into multi-step model predictive control framework to achieve better performance in terms of system

stability and robustness, which may involve further convexification across multiple time steps. Other applications of the SDP formulation will also be considered, such as market-based DR bidding strategy development, net-zero emission buildings with rooftop solar and storage systems.

VII. Conclusion

This paper proposes an optimization-based real-time HVAC flexibility quantification framework. The core of the proposed framework is an SDP formulation derived from the non-convex optimization problem of HVAC power minimization under normal conditions. The flexibility of HVAC under different operation conditions can be quantified and summarized into a flexibility table. The optimal response strategy in response to DR events can be found within the table to achieve the minimum cost of occupant comfort while satisfying grid requirements. Numerical results show that the HVAC flexibility table provides clear guidance on the range of feasible power reduction that can be achieved at each time step and the setpoints that should be adopted. The critical points in the table also provide information about adjustment boundaries. Moreover, with the addition of supply air temperature adjustment, the room temperature deviation can be reduced effectively and the maximum flexibility can be increased as well. The future work will consider multi-time-step SDP which will convexify the nonlinear terms between adjacent time steps. Also, the proposed SDP formulation can potentially be used for finding the optimal bidding strategies of demand-side resources in energy markets.

Disclaimer: The views expressed herein do not necessarily represent the views of the U.S. Department of Energy or the United States Government.

Appendix A
Analytic Solution of Pump Power Model Quadratic Approximation

The project theorem is applied to find the approximated coefficients γ_0, γ_1, and γ_2 that minimize the error $\|P_p - \hat{P}_p\|$. According to the theorem, $\|P_p - \hat{P}_p\|$ is the minimum when it is perpendicular to the projected space, as formulated in (20).

$$\langle P_p - \hat{P}_p, \hat{P}_p \rangle = 0 \tag{20}$$

Expanding the inner product, we get (21).

$$\int_{\underline{\dot{m}}_{sw}}^{\overline{\dot{m}}_{sw}} \left(P_p - \hat{P}_p\right) \hat{P}_p \, d\dot{m}_{sw} = 0 \tag{21}$$

where P_p and $\hat{P}_p$ are both functions of $\dot{m}_{sw}$. The upper and lower limit of integral, $\overline{\dot{m}}_{sw}$ and $\underline{\dot{m}}_{sw}$, are constants that denote the approximation range. Inserting (2) and (11) to (21) we get (22). Calculating the integral, (22) becomes (23), which can be organized into a compact matrix form (24), where $A = [\hat{\gamma}_0, \hat{\gamma}_1, \hat{\gamma}_2]^T$, $M \in \mathbb{R}^{3\times 3}$ is the symmetrical matrix in (25), and $d \in \mathbb{R}^3$ is the vector in (26).

Now the solution of the approximated coefficient vector A can be analytically solved as in (27).

$$A = \left(-d^T M^{-1}\right)^T \tag{27}$$

$$\int_{\underline{\dot{m}}_{sw}}^{\overline{\dot{m}}_{sw}} \begin{pmatrix} \gamma_3\hat{\gamma}_2\dot{m}_{sw}^5 + \left[\left(\gamma_2 - \hat{\gamma}_2\right)\hat{\gamma}_2 + \gamma_3\hat{\gamma}_1\right]\dot{m}_{sw}^4 \\ + \left[\left(\gamma_1 - \hat{\gamma}_1\right)\hat{\gamma}_2 + \left(\gamma_2 - \hat{\gamma}_2\right)\hat{\gamma}_1 + \gamma_3\hat{\gamma}_0\right]\dot{m}_{sw}^3 \\ + \left[\left(\gamma_0 - \hat{\gamma}_0\right)\hat{\gamma}_2 + \left(\gamma_1 - \hat{\gamma}_1\right)\hat{\gamma}_1 + \left(\gamma_2 - \hat{\gamma}_2\right)\hat{\gamma}_0\right]\dot{m}_{sw}^2 \\ + \left[\left(\gamma_0 - \hat{\gamma}_0\right)\hat{\gamma}_1 + \left(\gamma_1 - \hat{\gamma}_1\right)\hat{\gamma}_0\right]\dot{m}_{sw} \\ + \left(\gamma_0 - \hat{\gamma}_0\right)\hat{\gamma}_0 \end{pmatrix} d\dot{m}_{sw} = 0 \tag{22}$$

$$\begin{pmatrix} -\left(\overline{\dot{m}}_{sw} - \underline{\dot{m}}_{sw}\right)\hat{\gamma}_0^2 - \frac{1}{3}\left(\overline{\dot{m}}_{sw}^3 - \underline{\dot{m}}_{sw}^3\right)\hat{\gamma}_1^2 - \frac{1}{5}\left(\overline{\dot{m}}_{sw}^5 - \underline{\dot{m}}_{sw}^5\right)\hat{\gamma}_2^2 \\ -\left(\overline{\dot{m}}_{sw}^2 - \underline{\dot{m}}_{sw}^2\right)\hat{\gamma}_0\hat{\gamma}_1 - \frac{2}{3}\left(\overline{\dot{m}}_{sw}^3 - \underline{\dot{m}}_{sw}^3\right)\hat{\gamma}_0\hat{\gamma}_2 - \frac{1}{2}\left(\overline{\dot{m}}_{sw}^4 - \underline{\dot{m}}_{sw}^4\right)\hat{\gamma}_1\hat{\gamma}_2 \\ + \left[\gamma\left(\overline{\dot{m}}_{sw} - \underline{\dot{m}}_{sw}\right) + \frac{\gamma_1}{2}\left(\overline{\dot{m}}_{sw}^2 - \underline{\dot{m}}_{sw}^2\right) + \frac{\gamma_2}{3}\left(\overline{\dot{m}}_{sw}^3 - \underline{\dot{m}}_{sw}^3\right) + \frac{\gamma_3}{4}\left(\overline{\dot{m}}_{sw}^4 - \underline{\dot{m}}_{sw}^4\right)\right]\hat{\gamma}_0 \\ + \left[\frac{\gamma_0}{2}\left(\overline{\dot{m}}_{sw}^2 - \underline{\dot{m}}_{sw}^2\right) + \frac{\gamma_1}{3}\left(\overline{\dot{m}}_{sw}^3 - \underline{\dot{m}}_{sw}^3\right) + \frac{\gamma_2}{4}\left(\overline{\dot{m}}_{sw}^4 - \underline{\dot{m}}_{sw}^4\right) + \frac{\gamma_3}{5}\left(\overline{\dot{m}}_{sw}^5 - \underline{\dot{m}}_{sw}^5\right)\right]\hat{\gamma}_1 \\ + \left[\frac{\gamma_0}{3}\left(\overline{\dot{m}}_{sw}^3 - \underline{\dot{m}}_{sw}^3\right) + \frac{\gamma_1}{4}\left(\overline{\dot{m}}_{sw}^4 - \underline{\dot{m}}_{sw}^4\right) + \frac{\gamma_2}{5}\left(\overline{\dot{m}}_{sw}^5 - \underline{\dot{m}}_{sw}^5\right) + \frac{\gamma_3}{6}\left(\overline{\dot{m}}_{sw}^6 - \underline{\dot{m}}_{sw}^6\right)\right]\hat{\gamma}_2 \end{pmatrix} = 0 \tag{23}$$

$$A^T M A + d^T A = 0 \tag{24}$$

$$M = \begin{bmatrix} -\left(\overline{\dot{m}}_{sw} - \underline{\dot{m}}_{sw}\right) & -\frac{1}{2}\left(\overline{\dot{m}}_{sw}^2 - \underline{\dot{m}}_{sw}^2\right) & -\frac{1}{3}\left(\overline{\dot{m}}_{sw}^3 - \underline{\dot{m}}_{sw}^3\right) \\ -\frac{1}{2}\left(\overline{\dot{m}}_{sw}^2 - \underline{\dot{m}}_{sw}^2\right) & -\frac{1}{3}\left(\overline{\dot{m}}_{sw}^3 - \underline{\dot{m}}_{sw}^3\right) & -\frac{1}{4}\left(\overline{\dot{m}}_{sw}^4 - \underline{\dot{m}}_{sw}^4\right) \\ -\frac{1}{3}\left(\overline{\dot{m}}_{sw}^3 - \underline{\dot{m}}_{sw}^3\right) & -\frac{1}{4}\left(\overline{\dot{m}}_{sw}^4 - \underline{\dot{m}}_{sw}^4\right) & -\frac{1}{5}\left(\overline{\dot{m}}_{sw}^5 - \underline{\dot{m}}_{sw}^5\right) \end{bmatrix} \tag{25}$$

$$d = \begin{bmatrix} \gamma_0\left(\overline{\dot{m}}_{sw} - \underline{\dot{m}}_{sw}\right) + \frac{\gamma_1}{2}\left(\overline{\dot{m}}_{sw}^2 - \underline{\dot{m}}_{sw}^2\right) + \frac{\gamma_2}{3}\left(\overline{\dot{m}}_{sw}^3 - \underline{\dot{m}}_{sw}^3\right) + \frac{\gamma_3}{4}\left(\overline{\dot{m}}_{sw}^4 - \underline{\dot{m}}_{sw}^4\right) \\ \frac{\gamma_0}{2}\left(\overline{\dot{m}}_{sw}^2 - \underline{\dot{m}}_{sw}^2\right) + \frac{\gamma_1}{3}\left(\overline{\dot{m}}_{sw}^3 - \underline{\dot{m}}_{sw}^3\right) + \frac{\gamma_2}{4}\left(\overline{\dot{m}}_{sw}^4 - \underline{\dot{m}}_{sw}^4\right) + \frac{\gamma_3}{5}\left(\overline{\dot{m}}_{sw}^5 - \underline{\dot{m}}_{sw}^5\right) \\ \frac{\gamma_0}{3}\left(\overline{\dot{m}}_{sw}^3 - \underline{\dot{m}}_{sw}^3\right) + \frac{\gamma_1}{4}\left(\overline{\dot{m}}_{sw}^4 - \underline{\dot{m}}_{sw}^4\right) + \frac{\gamma_2}{5}\left(\overline{\dot{m}}_{sw}^5 - \underline{\dot{m}}_{sw}^5\right) + \frac{\gamma_3}{6}\left(\overline{\dot{m}}_{sw}^6 - \underline{\dot{m}}_{sw}^6\right) \end{bmatrix} \tag{26}$$

APPENDIX B PROOF OF REDUNDANCY

By $W \succcurlyeq 0$, we have $det(W) \geq 0$. (28a) expands the $det(W)$ according to the Laplace expansion [37]. Then, we substitute (17e), (17f), and (17g) into (28a) and get $det(W)$ equals (28d), which turned out to be a negative semidefinite equation.

$$det(W) = W_{11}W_{22}W_{33} + W_{21}W_{32}W_{13} + W_{12}W_{23}W_{31} - W_{13}W_{22}W_{31} - W_{12}W_{21}W_{33} - W_{23}W_{32}W_{11} \tag{28a}$$

$$= W_{13}^2W_{23}^2 + 2W_{12}W_{13}W_{23} - W_{13}^2W_{23}^2 - W_{12}^2 - W_{11}W_{23}^2 \tag{28b}$$

$$= 2W_{12}W_{13}W_{23} - W_{12}^2 - W_{13}^2W_{23}^2 \tag{28c}$$

$$= -(W_{12} - W_{13}W_{23})^2 \tag{28d}$$

It means, if there exists a feasible solution of W, $det(W)$ must be equal to zero, i.e., $(W_{12} - W_{13}W_{23})^2 = 0$, which is equivalent to $W_{12} = W_{13}W_{23}$. Therefore (17h) must hold when both (17f) and (17g) are true.

REFERENCES

[1] R. Bessa, C. Moreira, B. Silva, and M. Matos, "Handling renewable energy variability and uncertainty in power systems operation," *Wiley Interdiscipl. Reviews: Energy Environ.*, vol. 3, no. 2, pp. 156–178, 2014.

[2] I. Beil, I. Hiskens, and S. Backhaus, "Frequency regulation from commercial building HVAC demand response," *Proc. IEEE*, vol. 104, no. 4, pp. 745–757, 2016.

[3] B. Sivaneasan, N. K. Kandasamy, M. L. Lim, and K. P. Goh, "A new demand response algorithm for solar PV intermittency management," *Appl. Energy*, vol. 218, pp. 36–45, 2018.

[4] Y. Lin, P. Barooah, S. Meyn, and T. Middelkoop, "Experimental evaluation of frequency regulation from commercial building HVAC systems," *IEEE Trans. Smart Grid*, vol. 6, no. 2, pp. 776–783, Mar. 2015.

[5] A. Hassan, R. Mieth, D. Deka, and Y. Dvorkin, "Stochastic and distributionally robust load ensemble control," *IEEE Trans. Power Syst.*, vol. 35, no. 6, pp. 4678–4688, Nov. 2020.

[6] EIA, "How much energy is consumed in U.S. residential and commercial buildings?," FAQ - U.S. Energy Information Administration (EIA). [Online]. Available: https://www.eia.gov/tools/faqs/faq.php?id=86&t=1, Accessed on: Mar. 06, 2021.

[7] J. L. Mathieu, P. N. Price, S. Kiliccote, and M. A. Piette, "Quantifying changes in building electricity use, with application to demand response," *IEEE Trans. Smart Grid*, vol. 2, no. 3, pp. 507–518, Sep. 2011.

[8] P. Mancarella and G. Chicco, "Real-time demand response from energy shifting in distributed multi-generation," *IEEE Trans. Smart Grid*, vol. 4, no. 4, pp. 1928–1938, Dec. 2013.

[9] T. Adefarati and R. Bansal, "Reliability assessment of distribution system with the integration of renewable distributed generation," *Appl. Energy*, vol. 185, pp. 158–171, 2017.

[10] N. Lu, "An evaluation of the HVAC load potential for providing load balancing service," *IEEE Trans. Smart Grid*, vol. 3, no. 3, pp. 1263–1270, Sep. 2012.

[11] A. Coffman, Z. Guo, and P. Barooah, "Characterizing capacity of flexible loads for providing grid support," *IEEE Trans. Power Syst.*, vol. 36, no. 3, pp. 2428–2437, May 2021.

[12] Y. Ma, F. Borrelli, B. Hencey, B. Coffey, S. Bengea, and P. Haves, "Model predictive control for the operation of building cooling systems," *IEEE Trans. Control Syst. Technol.*, vol. 20, no. 3, pp. 796–803, May 2012.

[13] M. Ostadijafari and A. Dubey, "Linear model-predictive controller (LMPC) for building's heating ventilation and air conditioning (HVAC) system," in *Proc. IEEE Conf. Control Technol. Appl.*, 2019, pp. 617–623.

[14] J. Rehrl and M. Horn, "Temperature control for HVAC systems based on exact linearization and model predictive control," in *Proc. IEEE Int. Conf. Control Appl.*, 2011, pp. 1119–1124.

[15] G. Tian, S. Faddel, Q. Zhou, Z. Qu, and A. Parlato, "Optimal coordination of HVAC scheduling for commercial buildings," in *Proc. IEEE Texas Power Energy Conf.*, 2020, pp. 1–5.

[16] J. Drgoňa *et al.*, "All you need to know about model predictive control for buildings," *Annu. Rev. Control*, vol. 50, pp. 190–232, 2020.

[17] I. Hussain, S. Mohsin, A. Basit, Z. A. Khan, U. Qasim, and N. Javaid, "A review on demand response: Pricing, optimization, and appliance scheduling," *Procedia Comput. Sci.*, vol. 52, pp. 843–850, 2015.

[18] W. Mai and C. Chung, "Economic MPC of aggregating commercial buildings for providing flexible power reserve," *IEEE Trans. Power Syst.*, vol. 30, no. 5, pp. 2685–2694, Sep. 2015.

[19] D. T. Vedullapalli, R. Hadidi, and B. Schroeder, "Combined HVAC and battery scheduling for demand response in a building," *IEEE Trans. Ind. Appl.*, vol. 55, no. 6, pp. 7008–7014, Nov./Dec. 2019.

[20] Y. Yao and D. K. Shekhar, "State of the art review on model predictive control (MPC) in heating ventilation and air-conditioning (HVAC) field," *Building Environ.*, vol. 205, 2021, Art. no. 107952.

[21] M. Avci, M. Erkoc, A. Rahmani, and S. Asfour, "Model predictive HVAC load control in buildings using real-time electricity pricing," *Energy Buildings*, vol. 60, pp. 199–209, 2013.

[22] B. Kocuk, S. S. Dey, and X. A. Sun, "Strong SOCP relaxations for the optimal power flow problem," *Operations Res.*, vol. 64, no. 6, pp. 1177–1196, 2016.

[23] R. Yin *et al.*, "Quantifying flexibility of commercial and residential loads for demand response using setpoint changes," *Appl. Energy*, vol. 177, pp. 149–164, 2016.

[24] S. Huang, Y. Ye, D. Wu, and W. Zuo, "An assessment of power flexibility from commercial building cooling systems in the United States," *Energy*, vol. 221, 2021, Art. no. 119571.

[25] W. Tian, Y. Fu, Q. Wang, T. A. Sevilla, and W. Zuo, "Optimization on thermostat location in an office room using the coupled simulation platform in modelica buildings library: A pilot study," in *Proc. 4th Int. Conf. Building Energy Environ.*, 2018, pp. 1–6.

[26] F. Jorissen, W. Boydens, and L. Helsen, "Model implementation and verification of the envelope, HVAC and controller of an office building in modelica," *J. Building Perform. Simul.*, vol. 12, no. 4, pp. 445–464, 2019.

[27] M. Trčka and J. L. Hensen, "Overview of HVAC system simulation," *Automat. Construction*, vol. 19, no. 2, pp. 93–99, 2010.

[28] R. Adhikari, M. Pipattanasomporn, and S. Rahman, "Heuristic algorithms for aggregated HVAC control via smart thermostats for regulation service," *IEEE Trans. Smart Grid*, vol. 11, no. 3, pp. 2023–2032, May 2020.

[29] M. Cai, S. Ramdaspalli, M. Pipattanasomporn, S. Rahman, A. Malekpour, and S. R. Kothandaraman, "Impact of HVAC set point adjustment on energy savings and peak load reductions in buildings," in *Proc. IEEE Int. Smart Cities Conf.*, 2018, pp. 1–6.

[30] M. Stewart, *Surface Production Operations: Volume IV: Pumps and Compressors*. Houston, TX, USA: Gulf Professional Publishing, 2018.

[31] M. Hydeman, K. L. Gillespie, and A. Dexter, "Tools and techniques to calibrate electric chiller component models," *ASHRAE Trans.*, vol. 108, no. 1, pp. 733–741, 2002.

[32] M. Lauster, J. Teichmann, M. Fuchs, R. Streblow, and D. Mueller, "Low order thermal network models for dynamic simulations of buildings on city district scale," *Building Environ.*, vol. 73, pp. 223–231, 2014.

[33] N. S. Raman, K. Devaprasad, B. Chen, H. A. Ingley, and P. Barooah, "Model predictive control for energy-efficient HVAC operation with humidity and latent heat considerations," *Appl. Energy*, vol. 279, 2020, Art. no. 115765.

[34] M. Gouda, S. Danaher, and C. Underwood, "Building thermal model reduction using nonlinear constrained optimization," *Building Environ.*, vol. 37, no. 12, pp. 1255–1265, 2002.

[35] M. Alhaider and L. Fan, "Planning energy storage and photovoltaic panels for demand response with heating ventilation and air conditioning systems," *IEEE Trans. Ind. Informat.*, vol. 14, no. 11, pp. 5029–5037, Nov. 2018.

[36] Z. Yu, L. Jia, M. C. Murphy-Hoye, A. Pratt, and L. Tong, "Modeling and stochastic control for home energy management," *IEEE Trans. Smart Grid*, vol. 4, no. 4, pp. 2244–2255, Dec. 2013.

[37] D. Poole, *Linear Algebra: A Modern Introduction*. Boston, MA, USA: Nelson Education, 2014.

Guanyu Tian (Graduate Student Member, IEEE) received the B.Sc. degree in electrical engineering from Shandong University, Jinan, China, in 2015, and the M.S. degree in electrical engineering from Rensselaer Polytechnic Institute, Troy, NY, USA, in 2016. He is currently working toward the Ph.D. degree with the University of Central Florida, Orlando, FL, USA. His research interests include modeling and optimization of energy systems, demand response, and state estimation.

Qun Zhou Sun (Member, IEEE) received the Ph.D. degree in electrical engineering from Iowa State University, Ames, IA, USA. She is currently an Assistant Professor with the University of Central Florida (UCF), Orlando, FL, USA. She is the Director of UCF Smart Infrastructure Data Analytics Lab. Before joining UCF, she was with Genscape and GE Grid Solutions, as a Power System Engineer. She is devoted to improving energy efficiency and customer engagement through data analytics, probabilistic modeling, and advanced pricing schemes. She focuses on grid-edge resources, including smart buildings, rooftop PVs, and batteries, and their interactions with the grid.

Wenyi Wang received the B.S. degree in heating, ventilation, and air conditioning (HVAC) from the Xi'an University of Architecture and Technology, Xi'an, China, in 2007, the M.S degree in power engineering and engineering thermopyhsics from Xi'an Jiaotong University, Xi'an, China, in 2012, and the Ph.D. degree in mechanical engineering from the University of Texas at Dallas, Dallas, TX, USA, in 2019. He is currently a Postdoctoral with the Department of Electrical and Computer Engineering, University of Central Frolira, Orlando, FL, USA. His research interests include smart buildings, HVAC system modeling, optimization, and smart grid.